Stress intensity factor analysis of a three-dimensional interfacial corner between anisotropic bimaterials under thermal stress

Nomura, Yoshiaki; Ikeda, Toru; Miyazaki, Noriyuki

Title

Stress Intensity Factor Analysis of a Three-dimensional Interfacial Corner between Anisotropic Bimaterials under Thermal Stress

Authors

Yoshiaki Nomura, Toru Ikeda and Noriyuki Miyazaki

Affiliations

Department of Mechanical Engineering and Science, Kyoto University, Yoshida-Honmachi, Sakyo-ku, Kyoto, 606-8501, Japan.

Abstract

A numerical method using a path-independent *H*-integral based on the conservation integral was developed to analyze the singular stress field of a three-dimensional interfacial corner between anisotropic bimaterials under thermal stress. In the present method, the shape of the corner front is smooth. According to the theory of linear elasticity, asymptotic stress near the tip of a sharp interfacial corner is generally singular as a result of a mismatch of the materials' elastic constants. The eigenvalues and the eigenfunctions are obtained using the Williams eigenfunction method, which depends on the anisotropic materials' properties and the geometry of an interfacial corner. The order of the singularity related to the eigenvalue is real, complex or power-logarithmic. The amplitudes of the singular stress terms can be calculated using the *H*-integral. The stress and displacement around an interfacial corner for the *H*-integral are obtained using finite element analysis. In this study, a proposed definition of the stress intensity factors of an interfacial corner, which includes those of an interfacial crack and a homogeneous crack, is used to evaluate the singular stress fields. Asymptotic solutions of stress and displacement around an interfacial corner front are uniquely obtained using these stress intensity factors. To prove the accuracy of the present method, several different kinds of examples are shown such as interfacial corners or cracks in three-dimensional structures.

Keywords

H-integral, Stress Singularity, Interfacial Corner, Anisotropic, Thermal Stress, Stress Intensity Factor, Stroh Formalism, Finite Element Method

Main Text

1. Introduction

Micro-structures such as those utilized in electronic devices and micro-electro mechanical systems (MEMS) are composed of many different materials. Many interfacial corners exist in electronic devices and MEMS because each of the materials employed has a different configuration. Due to the mismatch of the materials' thermal expansion and elastic properties, the stress concentration at an interfacial corner may cause failure. Therefore, the strength of an interfacial corner is very important for the reliability of an electronic product.

Singular stress fields usually occur near the tip of a sharp interfacial corner, and they have been investigated in a number of studies. For two-dimensional problems, Williams (1952) used an eigenvalue approach on a corner in homogeneous media, with this method expanded in a later paper (1957). Stern et al. (1976), Sinclair et al. (1984), Carpenter (1984) and Babuska and Miller (1984) employed Betti's reciprocal principle to derive the path-independent *H*-integral and applied this integral to a corner in an isotropic, homogeneous media for the calculation of stress intensities. This approach was extended to a corner involving dissimilar isotropic materials by Carpenter and Byers (1987) and to thermal elastic problems by Banks-Sills and Ishbir (1997, 2004). Using the Stroh formalism (Stroh, 1958; Ting, 1996) and the *H*-integral, asymptotic solutions to stress and displacement near the corner of dissimilar anisotropic materials have been computed by Labossiere and Dunn (1999). A general solution for the eigenvalues of anisotropic multi-material corners has been provided by Hwu et al. (2003) including non-degeneretae materials, and by Barroso et al. (2003) and Yin (2003), including both degenerate and non-degenerate materials. Hartraft and Sih (1967) described additional eigenvalues and eigen-functions for a three-dimensional crack in a homogeneous isotropic material. Omer et al. (2004) and Yosibash et al. (2005) investigated the additional eigenvalues and eigen-functions of so-called "shadows" for three-dimensional polyhedral domains of isotropic materials in the vicinity of an edge.

The *H*-integral was applied to a wedge corner that consists of general anisotropic multi-materials, and the unified definition of stress intensity factors of such a corner was proposed by Hwu and Kuo

(2007). For three-dimensional problems, the *H*-integral was extended to the domain integral and applied to a straight corner in an isotropic, homogeneous structure by Ortiz et al. (2006). Although many studies have clarified the issues of three-dimensional crack problems, three-dimensional corner problems are still a relatively unexplored area of study.

In the present paper, we propose a new numerical method to analyze asymptotic stress and displacement fields around a smooth-fronted three-dimensional interfacial corner between dissimilar anisotropic materials under thermal stress. By using the Williams eigenfunction expansion method, the Stroh formalism and the *H*-integral extended to three-dimensional thermoelastic problems, we can calculate asymptotic solutions near an interfacial corner. Since the stress intensities around the corner tip are generally mixed-mode, the proposed definition of stress intensity factors corresponding to the three deformation modes through the mode separation from asymptotic stresses is used to evaluate the singular stress fields (Nomura et al., 2009). These three stress intensity factors can lead to a precise asymptotic solution of stresses and displacements and are directly connected to those of interfacial cracks proposed by Hwu (1993) and of homogeneous cracks.

2. Singular stress and displacement fields near the tip of corner

Consider the three-dimensional (3-D) wedge corner that consists of *n* different anisotropic elastic materials as shown in Fig. 1(a). The index *k* represents the wedge number in a multi-material corner. Let (x_1, x_2, x_3) be the local rectangular coordinate system defined in the following way: the origin is located on the corner tip and the x_3-axis coincides with the tangent vector of the corner front as shown in Fig 1(b). In the x_1-x_2 plane, let (r,θ) be the polar coordinate system. The asymptotic solutions near the tip of a corner under thermal stress have been expressed as (Labossiere and Dunn, 1999; Banks-Sills and Ishbir, 2004):

$$\begin{aligned}\sigma_{ij}^{k}(r,\theta) &= \sum_{m=1}^{\mathrm{N}} C_m r^{\lambda_m - 1} f_{ij}^{mk}(\theta) + \sigma_{ij0}^{k}(r,\theta) \\ u_i^{k}(r,\theta) &= \sum_{m=1}^{\mathrm{N}} C_m r^{\lambda_m} g_i^{mk}(\theta) + u_{i0}^{k}(r,\theta)\end{aligned} \quad , \qquad (1)$$

where C_m (m=I,II, … N) are scalar coefficients obtained by the *H*-integral, λ_m are the eigenvalues (λ_m–1 is the order of the singularity), N is the number of the singular terms, f_{ij}^{mk} and g_i^{mk} are eigenfunctions related to each eigenvalue λ_m which depends upon angle θ. The last terms σ_{ij0}^{k} and u_{i0}^{k} are the regular stress and displacement components, respectively. The general solutions for

the eigenvalues and eigenfunctions of general anisotropic multi-bonded materials have been provided by Hwu et al. (2003). By employing the Stroh formalism (Stroh, 1958; Ting, 1996), the general solutions near the tip are expressed as

$$\begin{aligned}\mathbf{u}_k &= r^{\lambda}\{\mathbf{A}_k\langle\hat{\mu}_{jk}^{\lambda}(\theta)\rangle\mathbf{c}_k + \overline{\mathbf{A}}_k\langle\overline{\hat{\mu}}_{jk}^{\lambda}(\theta)\rangle\mathbf{d}_k\}\\ \mathbf{t}_k &= \lambda r^{\lambda-1}\{\mathbf{B}_k\langle\hat{\mu}_{jk}^{\lambda}(\theta)\rangle\mathbf{c}_k + \overline{\mathbf{B}}_k\langle\overline{\hat{\mu}}_{jk}^{\lambda}(\theta)\rangle\mathbf{d}_k\}\end{aligned} \tag{2}$$

$$\hat{\mu}_{jk}(\theta) = \cos\theta + \mu_{jk}\sin\theta, \quad j = 1,\ 2,\ 3\ , \tag{3}$$

where $\mathbf{t}$ is the traction vector related to stresses through $t_i = \sigma_{ij}n_j$ in which n_j denotes the normal vector of the boundary, $\mathbf{A}$ and $\mathbf{B}$ are 3 x 3 complex matrices composed of Stroh's eigenvectors, and μ_j is Stroh's eigenvalue. These eigenvectors and eigenvalues are functions of the anisotropic elastic constants for each material. $\mathbf{c}_k$ and $\mathbf{d}_k$ are complex coefficient vectors to be determined through the satisfaction of boundary conditions. The angular brackets < > stand for the 3 x 3 diagonal matrix, and the overbar denotes the conjugate of a complex number. Both the 1st and the nth materials have a traction-free boundary condition on their corner flanks, and the tractions and displacements are continuous across each interface at $\theta = \theta_1, \theta_2, \ldots, \theta_n$ shown in Fig. 1(a). These boundary conditions can be written as

$$\begin{aligned}\mathbf{t}_1(\theta_0) = \mathbf{t}_n(\theta_n) = \mathbf{0}\\ \mathbf{t}_k(\theta_k) = \mathbf{t}_{k+1}(\theta_k),\ \mathbf{u}_k(\theta_k) = \mathbf{u}_{k+1}(\theta_k), \quad k = 1,\ 2,\ ....,\ n-1\end{aligned} \tag{4}$$

Substituting Eq.(2) into Eq.(4) and using the key matrix $\widehat{\mathbf{N}}$, the boundary conditions are simplified as

$$\mathbf{E}_3\mathbf{p}^* = \mathbf{0}, \qquad \mathbf{E} = \begin{bmatrix}\mathbf{E}_1 & \mathbf{E}_2\\ \mathbf{E}_3 & \mathbf{E}_4\end{bmatrix} = \prod_{k=1}^{n}\widehat{\mathbf{N}}_k^{\lambda}(\theta_{k-1},\theta_k) \tag{5}$$

where

$$\widehat{\mathbf{N}}_k^{\lambda}(\theta_{k-1},\theta_k) = \begin{bmatrix}\mathbf{A}_k & \overline{\mathbf{A}}_k\\ \mathbf{B}_k & \overline{\mathbf{B}}_k\end{bmatrix}\begin{bmatrix}\langle\hat{\mu}_{jk}^{\lambda}(\theta_{k-1})\hat{\mu}_{jk}^{-\lambda}(\theta_k)\rangle & \mathbf{0}\\ \mathbf{0} & \langle\overline{\hat{\mu}}_{jk}^{\lambda}(\theta_{k-1})\overline{\hat{\mu}}_{jk}^{-\lambda}(\theta_k)\rangle\end{bmatrix}\begin{bmatrix}\mathbf{B}_k^T & \mathbf{A}_k^T\\ \overline{\mathbf{B}}_k^T & \overline{\mathbf{A}}_k^T\end{bmatrix} \tag{6}$$

Here, $\widehat{\mathbf{N}}$ is a 6 x 6 complex matrix, $\mathbf{E}_3$ is one of the 3 x 3 sub-matrices of the 6 x 6 matrix $\mathbf{E}$ as shown in Eq. (5), and $\mathbf{p}^*$ is a complex vector related to $\mathbf{c}_k$ and $\mathbf{d}_k$. Therefore the eigenvalue can be obtained by

$$\|\mathbf{E}_3\| = 0 \tag{7}$$

In this case, Eq.(7) has an infinite number of possible solutions for λ_m. Since the displacements are finite, only positive solutions are permitted, $0 < \mathrm{Re}[\lambda]$, and singular stress terms are dominant near the tip of a corner $\mathrm{Re}[\lambda] < 1$. Thus we will focus only on the region

$$0 < \mathrm{Re}[\lambda] < 1 \tag{8}$$

Using λ_m obtained by Eq.(7) and key matrix $\widehat{\mathbf{N}}$, eigenfunctions $\mathbf{F}^{mk}$ and $\mathbf{g}^{mk}$ related to f_{ij}^{mk} and g_i^{mk} are expressed as

$$\begin{Bmatrix} \mathbf{g}^{mk}(\theta) \\ \mathbf{F}^{mk}(\theta) \end{Bmatrix} = \begin{cases} \widehat{\mathbf{N}}_k^{\lambda_m}(\theta,\theta_k)\prod_{i=k+1}^{n}\widehat{\mathbf{N}}_i^{\lambda_m}(\theta_{i-1},\theta_i)\begin{Bmatrix} \mathbf{p}^* \\ \mathbf{0} \end{Bmatrix}, k=1,2,\ldots,n-1 \\ \widehat{\mathbf{N}}_k^{\lambda_m}(\theta,\theta_k)\begin{Bmatrix} \mathbf{p}^* \\ \mathbf{0} \end{Bmatrix}, \quad k=n \end{cases} \quad (n \geq 2) \tag{9}$$

$\mathbf{F}^{mk}$ is the eigenfunction of the stress function ϕ^{mk} which is given by

$$\phi^{mk} = C_m r^{\lambda_m}\mathbf{F}^{mk}(\theta) \tag{10}$$

The stress function is related to the stresses by

$$\sigma_{i2} = \phi_{i,1}, \quad \sigma_{i1} = -\phi_{i,2}, \quad i = 1,\ 2,\ 3 \tag{11}$$

From Eqs.(10) and (11), f_{ij}^{mk} is obtained. $\mathbf{g}^{mk}$ and g_i^{mk} have the following relation.

$$\mathbf{g}^{mk}(\theta) = \begin{Bmatrix} g_1^{mk}(\theta) \\ g_2^{mk}(\theta) \\ g_3^{mk}(\theta) \end{Bmatrix} \tag{12}$$

In the singular terms, the only quantities in Eq.(1) that are not obtained are scalar coefficients C_m, which depend on far-field geometry and mechanical and thermal loading.

As mentioned in the introduction, Omer et al. (2004) and Yosibash et al. (2005) described additional eigenvalues, the so-called "shadow" eigenvalues, for three-dimensional polyhedrals in the vicinity of an edge. In this study, we assumed that the effect of the "shadow" eigenvalues could be ignored for the engineering evaluation. However, the effect of "shadow" eigenvalues on the singular stress field around an edge in three-dimensional joined anisotropic materials has not been investigated. This effect should be investigated in future research.

3. *H*-integral for 3-D thermoelastic problems

The path-independent integral for a two-dimensional (2-D) corner, or the *H*-integral, is based on Betti's reciprocal principle (Sokolnikoff 1956), and it is employed to calculate the stress intensities, which are usually mixed-mode for an interfacial corner. If we consider a linear elastic body subjected to two systems of surface forces, the actual field and the complementary one, then the *H*-integral is defined by

$$H = \int_C (\sigma_{ij}u_i^* - \sigma_{ij}^* u_i)n_j dC \quad , \tag{13}$$

where σ_{ij} and u_i are the actual stress and displacement, respectively, and σ_{ij}^* and u_i^* are the

complementary stress and displacement that satisfy the same equilibrium and constitutive relations as the actual fields. n_j is the normal vector of the boundary and C is the integral path surrounding an interfacial corner. Eq. (13) should be applied for each wedge k in Fig. 1, separately. However, the index k will be omitted for the sake of simplicity in this section. The H-integral for 2-D thermoelastic problems was developed by Banks-Sills and Ishbir (2004), and we extended it to the corner including anisotropic materials (Nomura et al.).

$$H = \int_C (\sigma_{ij} u_i^* - \sigma_{ij}^* u_i) n_j dC + \int_S \beta_{ij} \vartheta \varepsilon_{ij}^* dS \quad , \tag{14}$$

where β_{ij} $(= C_{ijks}\alpha_{ks})$ is the thermal modulus, ε_{ij}^* is the complementary strain and ϑ is the actual temperature.

From the original conservation integral, we developed the H-integral for 3-D thermoelastic problems to calculate the scalar coefficient C_m. For the static loading conditions, the constitutive and equilibrium relations and the strain-displacement relation can be written as

$$\sigma_{ij} = C_{ijks}\varepsilon_{ks} - \beta_{ij}\vartheta, \quad \sigma_{ij,j} = 0, \quad \varepsilon_{ij} = \frac{1}{2}(u_{i,j} + u_{j,i}) \tag{15}$$

In this condition, we consider a thermoelastic body subjected to two systems, the actual and the complementary. Then, we get the following conservation integral from Eq.$(15)_1$:

$$\int_V (\sigma_{ij}\varepsilon_{ij}^* - \sigma_{ij}^*\varepsilon_{ij}) dV + \int_V (\beta_{ij}\vartheta\varepsilon_{ij}^* - \beta_{ij}\vartheta^*\varepsilon_{ij}) dV = 0 \quad , \tag{16}$$

where V is any domain not containing the singular point. Substituting Eq.$(15)_3$ into the first term on the left-hand side of Eq.(16), and assuming that the stress is symmetric $(\sigma_{ij} = \sigma_{ji})$, Eq.(16) is written as

$$\int_V (\sigma_{ij} u_{i,j}^* - \sigma_{ij}^* u_{i,j}) dV + \int_V (\beta_{ij}\vartheta\varepsilon_{ij}^* - \beta_{ij}\vartheta^*\varepsilon_{ij}) dV = 0 . \tag{17}$$

The Gauss divergence theorem is applied to the first term on the left-hand side of Eq.(17) for each material wedge separately. The surface integral along an interface between different materials vanishes, according to the contribution from both materials. Then, considering the equilibrium relation Eq.$(15)_2$, we obtain

$$\int_S (\sigma_{ij} u_i^* - \sigma_{ij}^* u_i) n_j dS + \int_V (\beta_{ij}\vartheta\varepsilon_{ij}^* - \beta_{ij}\vartheta^*\varepsilon_{ij}) dV = 0 \quad , \tag{18}$$

where S is the closed-boundary surface of the domain V and n_j is the normal vector of the boundary S. The complementary solutions are chosen as the isothermal problem $(\vartheta^* = 0)$. Therefore, Eq.(18) becomes

$$\int_S (\sigma_{ij} u_i^* - \sigma_{ij}^* u_i) n_j dS + \int_V \beta_{ij} \vartheta \varepsilon_{ij}^* dV = 0 \quad . \tag{19}$$

If this conservation integral Eq.(19) is applied to the 3-D corner, the domain V is selected as shown in Fig. 2 and the surface S is selected to be $S_r + S_\delta + S_l + S_0 + S_1 + S_2$. S_r is the outer cylindrical surface of radius r, and S_δ is the inner cylindrical surface of small radius $\varepsilon > 0$. S_l and S_0 are the front and back surfaces parallel to the x_1-x_2 plane. S_1 and S_2 are the angle surfaces that contain the corner flanks at $x_3 = 0$. We assume a traction-free condition on S_1 and S_2 if the width l is selected to be small. The complementary solutions are taken so that they also satisfy the traction-free condition on S_1 and S_2. Hence, the surface integrals on S_1 and S_2 are zero, and Eq.(19) is written as

$$\begin{aligned} &\int_{S_r} (\sigma_{ij} u_i^* - \sigma_{ij}^* u_i) n_j dS + \int_{S_\delta} (\sigma_{ij} u_i^* - \sigma_{ij}^* u_i) n_j dS \\ &+ \int_{S_l} (\sigma_{ij} u_i^* - \sigma_{ij}^* u_i) n_j dS + \int_{S_0} (\sigma_{ij} u_i^* - \sigma_{ij}^* u_i) n_j dS + \int_V \beta_{ij} \vartheta \varepsilon_{ij}^* dV = 0 \end{aligned} \tag{20}$$

On S_l and S_0, the normal vectors are $(n_1\ n_2\ n_3) = (0\ 0\ 1)$ and $(0\ 0\ -1)$, respectively. We consider the surface S'_δ whose normal vector has the opposite direction to that of S_δ. Then, Eq.(20) becomes

$$\begin{aligned} &\int_{S'_\delta} (\sigma_{ij} u_i^* - \sigma_{ij}^* u_i) n_j dS = \\ &\int_{S_r} (\sigma_{ij} u_i^* - \sigma_{ij}^* u_i) n_j dS + \int_{S_l} (\sigma_{i3} u_i^* - \sigma_{i3}^* u_i) dS - \int_{S_0} (\sigma_{i3} u_i^* - \sigma_{i3}^* u_i) dS + \int_V \beta_{ij} \vartheta \varepsilon_{ij}^* dV \end{aligned} \tag{21}$$

Since the width l is very small, we assume that the integrands are constant with respect to x_3. Therefore, Eq.(21) can be written as

$$\begin{aligned} &l \int_{C'_\delta} (\sigma_{ij} u_i^* - \sigma_{ij}^* u_i) n_j dC = \\ &l \int_{C_r} (\sigma_{ij} u_i^* - \sigma_{ij}^* u_i) n_j dC + \int_{S_l} (\sigma_{i3} u_i^* - \sigma_{i3}^* u_i) dS - \int_{S_0} (\sigma_{i3} u_i^* - \sigma_{i3}^* u_i) dS + l \int_{S_0} \beta_{ij} \vartheta \varepsilon_{ij}^* dS \end{aligned} \tag{22}$$

where C'_δ and C_r are the circular contours of radii δ and r, respectively. If the width l approaches zero, and we choose the complementary stress and displacement to be constant with respect to x_3, we get

$$\int_{C'_\delta} (\sigma_{ij} u_i^* - \sigma_{ij}^* u_i) n_j dC = \int_{C_r} (\sigma_{ij} u_i^* - \sigma_{ij}^* u_i) n_j dC + \int_{S_0} (\sigma_{i3,3} u_i^* - \sigma_{i3}^* u_{i,3}) dS + \int_{S_0} \beta_{ij} \vartheta \varepsilon_{ij}^* dS \,. \tag{23}$$

When the radius of the inner contour is reduced, in the limit as $\delta \to 0$, H is defined as the integrand along C'_δ. Therefore, the path-independent H-integral is defined by

$$H = \int_{C_r} (\sigma_{ij} u_i^* - \sigma_{ij}^* u_i) n_j dC + \int_S (\sigma_{i3,3} u_i^* - \sigma_{i3}^* u_{i,3}) dS + \int_S \beta_{ij} \vartheta \varepsilon_{ij}^* dS \quad , \tag{24}$$

where the integral surface S is the area inside the contour C_r as shown in Fig. 3. The subscript k

denoting the materials has been neglected for simplicity. We integrated respective material k's regions individually in Eq. (24).

4. Interfacial corners between bimaterials

In this section, we consider an interfacial corner between anisotropic bimaterials as shown in Fig. 4, which shows a special case of a wedge corner consisting of two-bonded materials. The x_1-axis is placed in the interface. For an interfacial corner, the combination of the eigenvalues, calculation of the scalar coefficients by the H-integral, the moving least-square method and the definition of the stress intensity factors are treated.

4.1. Five combinations of the eigenvalues

Substituting $n = 2$, $k = A$ or B, $\theta_0 = -\beta$, $\theta_1 = 0$ and $\theta_2 = \alpha$ into Eqs.(5), (7) and (9), these equations are simplified as

$$\left\|\mathbf{E}_3\right\| = 0, \quad \mathbf{E} = \widehat{\mathbf{N}}_B^{\lambda}(-\beta,0)\widehat{\mathbf{N}}_A^{\lambda}(0,\alpha) \tag{25}$$

$$\begin{Bmatrix}\mathbf{g}^{mk}(\theta)\\ \mathbf{F}^{mk}(\theta)\end{Bmatrix} = \begin{cases}\widehat{\mathbf{N}}_B^{\lambda_m}(\theta,0)\widehat{\mathbf{N}}_A^{\lambda_m}(0,\alpha)\begin{Bmatrix}\mathbf{p}^*\\ \mathbf{0}\end{Bmatrix}, & (-\beta < \theta \le 0)\\ \widehat{\mathbf{N}}_A^{\lambda_m}(\theta,\alpha)\begin{Bmatrix}\mathbf{p}^*\\ \mathbf{0}\end{Bmatrix}, & (0 \le \theta < \alpha)\end{cases} \tag{26}$$

The eigenvalue obtained from Eq.(25) in the range of Eq.(8) may be real or complex. If the eigenvalue is a repeated root, the power-logarithmic stress singularities should be considered (Dempsey, 1995). Since few situations yield this singular behavior, the power-logarithmic type is not treated in the present study. The combination of the eigenvalue types depends upon the wedge angles (α, β) and the anisotropic elastic constants of the two materials. Hwu and Kuo (2007) classified the types of solutions by focusing on the most critical order. We assumed the following five (A-E) examples based on their classification system. We did not take other possible combinations of eigenvalues into account in this study.

(A) Three eigenvalues are real and non-repeated (N=3),

$$0 < \lambda_{\mathrm{I}} < \lambda_{\mathrm{II}} < \lambda_{\mathrm{III}} < 1 \tag{27}$$

(B) Two eigenvalues are real and non-repeated (N=2),

$$0 < \lambda_{\mathrm{I}} < \lambda_{\mathrm{II}} < 1 \tag{28}$$

(C) One eigenvalue is real and triple root (N=1),

$$\lambda_{\mathrm{I}} = 0.5 \tag{29}$$

(D) Two eigenvalues are complex and conjugate, one eigenvalue is real and non-repeated (N=3),

$$\begin{cases} \lambda_{\mathrm{I}} = \lambda + i\varepsilon,\ \lambda_{\mathrm{II}} = \lambda - i\varepsilon,\ \lambda_{\mathrm{III}} = \lambda', & \lambda \le \lambda' \\ \lambda_{\mathrm{I}} = \lambda',\ \lambda_{\mathrm{II}} = \lambda + i\varepsilon,\ \lambda_{\mathrm{III}} = \lambda - i\varepsilon, & \lambda > \lambda' \end{cases} \tag{30}$$

(E) Two eigenvalues are complex and conjugate (N=2),

$$\lambda_{\mathrm{I}} = \lambda + i\varepsilon,\ \lambda_{\mathrm{II}} = \lambda - i\varepsilon \tag{31}$$

where λ and ε are real numbers. Since the singular terms associated with λ_{I}, λ_{II} and λ_{III} are generally mixed-mode, the subscript of the eigenvalues has no relation with the three deformation modes. However, when the in-plane and anti-plane deformations can be decoupled, λ_m can be classified into in-plane and anti-plane eigenvalues. Then, regardless the order of eigenvalues according to Eqs.(25-29), λ_{III} is chosen to be the anti-plane eigenvalue, which is associated with anti-plane deformation, and the others (λ_{I}, λ_{II}) are the in-plane eigenvalues.

Type (C), which is the case of a crack in a homogeneous material, occurs if we set $\alpha = \beta = \pi$ and two identical materials $A = B$. In this case, three linearly independent $\mathbf{p}^*$ ($\mathbf{p}_1^*, \mathbf{p}_2^*, \mathbf{p}_3^*$) in Eq.(26) are selected since λ is a triple root. In spite of N = 1, three sets of f_{ij}^{mk} and g_i^{mk} corresponding to $\mathbf{p}_1^*, \mathbf{p}_2^*$, and $\mathbf{p}_3^*$ exist, and three scalar coefficients C_m are needed. In the other cases, the number of C_m needs to equal N. If the eigenvalue is complex, in the cases of (D) and (E), the corresponding scalar coefficient is also complex, so C_{I} and C_{II} or C_{II} and C_{III} are complex and conjugate.

4.2. Calculation of the scalar coefficients by H-integral

As the *H*-integral path C_r, a circular contour-clockwise path is selected for simplicity's sake as shown in Fig. 4. If the complementary solutions are chosen properly, *H* equals the scalar coefficient C_m. Szabo and Babuska (1988) and Wu and Chang (1993) showed that if λ_m is a solution of Eq.(25) , $-\lambda_m$ is also a solution. So we chose the complementary solutions as follows.

$$\begin{aligned} \sigma_{ij}^{k*} &= C_m^* r^{-\lambda_m - 1} f_{ij}^{mk*}(\theta) \\ u_i^{k*} &= C_m^* r^{-\lambda_m} g_i^{mk*}(\theta) \end{aligned} \tag{32}$$

$$\frac{1}{C_m^*} = \int_{-\beta}^{\alpha} (f_{ij}^{mk}(\theta) g_i^{mk*}(\theta) - f_{ij}^{mk*}(\theta) g_i^{mk}(\theta)) n_j d\theta \ , \tag{33}$$

where f_{ij}^{mk*} and g_i^{mk*} are obtained from Eq.(26) in the same way as f_{ij}^{mk} and g_i^{mk} are obtained. Superscript *k* represents the material *A* or *B*, according to the region where the variable belongs. These complementary solutions also satisfy the equilibrium and constitutive relations. By shrinking the inner path, the dominant contribution to the solutions inside the region comes from the singular terms. So, substituting Eqs.(1) and (32) into the *H*-integral of Eq.(23) with the limit as $\delta \to 0$, and using C^* given in Eq.(33), we obtain

$$H_m = \lim_{\delta \to 0} \int_{-\beta}^{\alpha} (\sigma_{ij}^k u_i^{k*} - \sigma_{ij}^{k*} u_i^k) n_j \delta d\theta = C_m \tag{34}$$

In the case of m = I, the singular stresses and displacements associated with the minimum eigenvalue λ_I of the actual field in Eq.(1) are of the order $O(\delta^{\lambda_I-1})$ and $O(\delta^{\lambda_I})$, respectively. Those of the complementary field in Eq.(32) are of the order $O(\delta^{-\lambda_I-1})$ and $O(\delta^{-\lambda_I})$. Therefore, the products of the above stresses and displacements expressed in Eq.(34) are of the order $O(\delta^{-1})$, and the other terms, whose orders are $O(\delta^{\lambda_{II}-\lambda_I})$ or $O(\delta^{\lambda_{III}-\lambda_I})$, are eliminated by $\delta \to 0$. Therefore, only the scalar coefficient C_I is left. In the same way, in the other cases in which m = II or III, the products of stresses and displacements associated with the eigenvalue λ_{II} *e.g.* in Eq.(1) and their complements are of the order $O(\delta^{-1})$, but the other terms whose order is $O(\delta^{\lambda_I-\lambda_{II}})$ cannot be eliminated by $\delta \to 0$. These terms are dissolved by the following relation:

$$\int_{-\beta}^{\alpha}(f_{ij}^{lk}(\theta)g_i^{mk*}(\theta)-f_{ij}^{mk*}(\theta)g_i^{lk}(\theta))n_j d\theta=0,\ \ l\neq m \tag{35}$$

Since the explicit expressions of f_{ij}^{mk}, g_i^{mk}, f_{ij}^{mk*} and g_i^{mk*} are also complicated, a rigorous proof is not easily performed. Instead, a numerical check has been done for all cases (A-E). In order to obtain all the scalar coefficients C_m, we need to evaluate the H-integral N times using the N patterns of Eqs.(32) and (33).

In the right-hand side of Eq.(24), the numerical solutions obtained using the finite element method are employed for the actual stress and displacement, and Eqs.(32) and (33) are used for the complementary values. Since complementary stress, strain and displacement in the surface integral on the right-hand side of Eq.(24) are of order $O(r^{-\lambda_m-1})$ or $O(r^{-\lambda_m})$, they are highly singular and cannot be integrated by standard numerical methods near the tip. To overcome this difficulty, the integral region is divided into the differential elements of area as shown in Fig. 5, and the analytic integration is carried out for a radial direction. When the integral path is circular, the element within the region is $rdrd\theta$, and if we assume that $\sigma_{i3,3}$, $u_{i,3}$, f_{ij}^{mk*}, g_i^{mk*} and ϑ in each element are constant in each element, the second and third terms of Eq.(24) can be rewritten as

$$\int_S(\sigma_{i3,3}u_i^*-\sigma_{i3}^*u_{i,3})rdrd\theta=C^*\sum_a\sum_b\left[\frac{\sigma_{i3,3}g_i^{m*}}{2-\lambda_m}(r_a^{2-\lambda_m}-r_{a-1}^{2-\lambda_m})-\frac{u_{i,3}f_{i3}^{m*}}{1-\lambda_m}(r_a^{1-\lambda_m}-r_{a-1}^{1-\lambda_m})\right](\theta_b-\theta_{b-1}) \tag{36}$$

$$\int_S\beta_{ij}\vartheta\varepsilon_{ij}^{m*}rdrd\theta=\frac{C^*}{1-\lambda_m}\sum_a\sum_b\alpha_{ij}\vartheta f_{ij}^{m*}(r_a^{1-\lambda_m}-r_{a-1}^{1-\lambda_m})(\theta_b-\theta_{b-1}), \tag{37}$$

where the subscript k has been neglected for the sake of simplicity. Using this method, we can avoid higher singular integration, which causes a large numerical error.

4.3. Moving least-square method

The moving least-square method (Lancaster and Salkauskas, 1989) is used as a pre-processing step of the H-integral. In many cases, data preparation for post-processing is troublesome. Therefore,

using the moving least-square method, the stress, strain and displacement used for the *H*-integral are approximated automatically based on nodal displacements obtained using the finite element method. The formulation of the moving least-square method is described as follows.

The approximation of displacement at an arbitrary point can be written as

$$\mathbf{u}^h(\boldsymbol{x}) = \mathbf{p}^T(\boldsymbol{x})\mathbf{a}(\boldsymbol{x}) \tag{38}$$

$$\mathbf{p}(\boldsymbol{x}) = \{1, x, y\}^T \tag{39}$$

$\mathbf{a}(\boldsymbol{x})$ is determined by minimizing the following weighted least-square form,

$$\mathbf{R}(\boldsymbol{x}) = \sum_I^n w(\boldsymbol{x}-\boldsymbol{x}_I)[\mathbf{p}^T(\boldsymbol{x}_I)\mathbf{a}(\boldsymbol{x}) - \mathbf{u}_I]^2 \ , \tag{40}$$

where $\mathbf{u}_I$ is the displacement at node I as shown in Fig. 6. The following exponential weight function was employed in this paper:

$$w(d_I) = \begin{cases} \dfrac{\exp(-(d_I/c)^2) - \exp(-(d_{mI}/c)^2)}{1-\exp(-(d_{mI}/c)^2)}, & \text{if } d_I \le d_{mI} \\ 0, & \text{if } d_I > d_{mI} \end{cases}, \tag{41}$$

where $d_I = \|\boldsymbol{x}-\boldsymbol{x}_I\|$, $c = \beta d_{mI}$, and β is a parameter which determines the sharpness of the weight function. $\mathbf{a}(\boldsymbol{x})$ is determined by taking the extremum of $\mathbf{R}(\boldsymbol{x})$, and by substituting $\mathbf{a}(\boldsymbol{x})$ into Eq.(38) to obtain

$$\mathbf{u}^h = \sum_I^n \sum_j^m p_j(\boldsymbol{x})[\mathbf{X}^{-1}(\boldsymbol{x})\mathbf{Y}(\boldsymbol{x})]_{jI}\mathbf{u}_I \equiv \sum_I^n \phi_I(\boldsymbol{x})\mathbf{u}_I \ , \tag{42}$$

where the shape function is given by

$$\phi_I(\boldsymbol{x}) = \sum_j^m p_j(\boldsymbol{x})[\mathbf{X}^{-1}(\boldsymbol{x})\mathbf{Y}(\boldsymbol{x})]_{jI} \tag{43}$$

$$\begin{aligned} &\mathbf{X}(\boldsymbol{x}) = \sum_I^n w(\boldsymbol{x}-\boldsymbol{x}_I)\mathbf{p}(\boldsymbol{x}_I)\mathbf{p}^T(\boldsymbol{x}_I) \\ &\mathbf{Y}(\boldsymbol{x}) = [w(\boldsymbol{x}-\boldsymbol{x}_1)\mathbf{p}(\boldsymbol{x}_1),\ w(\boldsymbol{x}-\boldsymbol{x}_2)\mathbf{p}(\boldsymbol{x}_2),\ \ldots w(\boldsymbol{x}-\boldsymbol{x}_I)\mathbf{p}(\boldsymbol{x}_I)] \end{aligned} \tag{44}$$

4.4. A definition of stress intensity factors

A unified definition of the stress intensity factors of an interfacial corner between anisotropic bimaterials has been proposed by Hwu and Kuo (2007), and it includes the definition of an interfacial crack (Hwu, 1993) and a crack in homogeneous material, as follows:

$$\mathbf{k} = \begin{Bmatrix} K_{\mathrm{II}} \\ K_{\mathrm{I}} \\ K_{\mathrm{III}} \end{Bmatrix} = \lim_{\substack{r\to 0 \\ \theta=0}} \sqrt{2\pi} r^{1-\mathrm{Re}[\lambda_1]} \mathbf{\Lambda}(\theta) \left\langle (r/l_k)^{-i\varepsilon_m} \right\rangle \mathbf{\Lambda}^{-1}(\theta) \begin{Bmatrix} \sigma_{12} \\ \sigma_{22} \\ \sigma_{32} \end{Bmatrix} \tag{45}$$

$$\mathbf{\Lambda}(\theta)=\left[\mathbf{F}^{\mathrm{I}}(\theta)\quad \mathbf{F}^{\mathrm{II}}(\theta)\quad \mathbf{F}^{\mathrm{III}}(\theta)\right]\ , \tag{46}$$

where l_k is a length parameter that may be chosen arbitrarily. However, since the stress intensity factors for different l_k values cannot be compared, the length parameter should be selected as a fixed value. **F** is obtained from Eq.(26), and < > stands for the 3 x 3 diagonal matrix, m=I, II, III .

In Eq. (45), only the smallest critical eigenvalue λ_{I} is considered, and the physical meaning of this definition is clear. When $r\to 0$, i.e., near the tip field, the term associated with λ_{I} will dominate the stress behavior. However, in the actual fracture, the terms associated with minor eigenvalues, λ_{II} and λ_{III}, may have considerable influence. Therefore, we propose a modified definition of the stress intensity factors for engineering applications, as follows:

$$\mathbf{k}=\begin{Bmatrix}K_{\mathrm{II}}\\K_{\mathrm{I}}\\K_{\mathrm{III}}\end{Bmatrix}=\lim_{\substack{r\to 0\\ \theta=0}}\sqrt{2\pi}\,l_k^{1-\mathrm{Re}[\lambda_{\mathrm{I}}]}\mathbf{\Lambda}(\theta)\left\langle (r/l_k)^{1-\lambda_m}\right\rangle\mathbf{\Lambda}^{-1}(\theta)\begin{Bmatrix}\sigma_{12}\\\sigma_{22}\\\sigma_{32}\end{Bmatrix}. \tag{47}$$

If the two eigenvalues exist, as in the cases of (B) and (E), the diagonal matrix and $\mathbf{\Lambda}$ are 2 x 2 and 3 x 2 matrices, respectively. In the case of Λ being a 3x2 matrix, one of the three modes is independent, and the matrix can be divided into a 2x2 matrix and a scalar value. Defined stress intensity factors have the dimension related to the smallest eigenvalue λ_{I}, because the stress intensity factors that have different dimensions are unified by the dominant dimension. The physical meaning of this definition is not as clear as that of the definition in Eq. (45); however, since the influence of all the singular terms can be reflected in the three stress intensity factors, K_{I}, K_{II} and K_{III}, it is convenient for use in actual facture evaluation. In our previous study (Nomura et al., 2009), we compared asymptotic solutions of stress near the tip of an interfacial corner obtained by the original and modified definitions. The asymptotic solution obtained by the modified stress intensity factors corresponded with the stress distribution around an interfacial corner in a wider region than that obtained by the original stress intensity factors.

Asymptotic solutions of stress and displacement near the tip of an interfacial corner are uniquely obtained using these stress intensity factors. For example, the stress ahead of an interfacial corner is expressed as

$$\begin{Bmatrix}\sigma_{12}\\\sigma_{22}\\\sigma_{32}\end{Bmatrix}=\frac{l_k^{\mathrm{Re}[\lambda_{\mathrm{I}}]-1}}{\sqrt{2\pi}}\mathbf{\Lambda}(0)\left\langle (r/l_k)^{\lambda_m-1}\right\rangle\mathbf{\Lambda}^{-1}(0)\begin{Bmatrix}K_{\mathrm{II}}\\K_{\mathrm{I}}\\K_{\mathrm{III}}\end{Bmatrix}+\begin{Bmatrix}\sigma_{120}\\\sigma_{220}\\\sigma_{320}\end{Bmatrix}\ . \tag{48}$$

Substituting the singular stress terms of Eq.(1) into Eq.(47), we obtain the relation between the scalar coefficient C_m and these stress intensity factors, as follows:

$$\begin{Bmatrix} K_{\mathrm{II}} \\ K_{\mathrm{I}} \\ K_{\mathrm{III}} \end{Bmatrix} = \sqrt{2\pi}\,[C_{\mathrm{I}} l_k^{\mathrm{Im}[\lambda_1]} \begin{Bmatrix} f_{12}^{\mathrm{I}}(0) \\ f_{22}^{\mathrm{I}}(0) \\ f_{32}^{\mathrm{I}}(0) \end{Bmatrix} + C_{\mathrm{II}} l_k^{\lambda_{\mathrm{II}} - \mathrm{Re}[\lambda_1]} \begin{Bmatrix} f_{12}^{\mathrm{II}}(0) \\ f_{22}^{\mathrm{II}}(0) \\ f_{32}^{\mathrm{II}}(0) \end{Bmatrix} + C_{\mathrm{III}} l_k^{\lambda_{\mathrm{III}} - \mathrm{Re}[\lambda_1]} \begin{Bmatrix} f_{12}^{\mathrm{III}}(0) \\ f_{22}^{\mathrm{III}}(0) \\ f_{32}^{\mathrm{III}}(0) \end{Bmatrix}] \tag{49}$$

In the cases of (B) and (E), the third term is absent. If l_k is changed to l_k', the relation of the stress intensity factors in Eq.(47) is written as

$$\mathbf{k}'(l_k') = \mathbf{\Lambda}(0)\left\langle (l_k / l_k')^{\mathrm{Re}[\lambda_1] - \lambda_m} \right\rangle \mathbf{\Lambda}^{-1}(0)\mathbf{k}(l_k) \tag{50}$$

5. Numerical results

The accuracy and efficiency of the present method has been examined for several interfacial corner or crack problems. Note that for all the examples, elastic analyses were carried out using the finite element method program. Twenty-noded isoparametric elements were used. The moving least-square method was used to determine stresses and displacements along circular paths around an interfacial corner. The length parameter l_k was selected to be 10μm.

5.1. A penny-shaped interfacial crack between dissimilar isotropic materials

As a benchmark, a penny-shaped interfacial crack with a diameter of $2a$ between infinite dissimilar isotropic media subjected to the remote tension σ_0 as shown in Fig. 7 was analyzed. In this case, there is no thermal loading. The analytical solution of the stress intensity factors was proposed by Kassir and Bregman (1972) as

$$K_{\mathrm{I}} + iK_{\mathrm{II}} = 2\sigma_0\sqrt{a}\,\frac{\Gamma(2+i\varepsilon)}{\Gamma(1/2+i\varepsilon)} \qquad \text{for} \quad l_k = 2a, \tag{51}$$

where Γ is the gamma function, and i is the complex constant $(i^2 = -1)$. When the reference length l_k is different from the crack length $2a$, like the example shown in Table 1, Eq. (50) is needed for the calculation of the corresponding stress intensity factors. Uniform stresses σ_1 and σ_2 along the outer wall (see Fig. 7) are required to satisfy the continuity of displacement along the interface, *i.e.*,

$$\sigma_2 = \frac{1}{1-\nu_2}\left[\frac{\mu_2}{\mu_1}(1-\nu_1)\sigma_1 + \left\{\nu_2 - \frac{\mu_2}{\mu_1}\nu_1\right\}\sigma_0\right] \tag{52}$$

where μ_j and ν_j are the shear modulus and Poisson's ratio of material j, respectively.

Due to the symmetric geometry, one-quarter of the problem was modeled as shown in Fig. 7. Young's moduli and Poisson's ratios were set to be E_1 = 150 GPa, E_2 = 20 GPa, and ν_1 = 0.30, ν_2 = 0.25, respectively. The corresponding bimaterial constant is ε = –0.08552; therefore, the eigenvalues are $\lambda_{\mathrm{I}} = 0.5+i\varepsilon$, $\lambda_{\mathrm{II}} = 0.5-i\varepsilon$ and $\lambda_{\mathrm{III}} = 0.5$. The remote tension ($\sigma_0$) was 10 MPa. The number of nodes and elements of the FE mesh were 131,239 and 30,770, respectively. The size of the smallest elements was 1/20 of the crack radius a (10mm). The relative errors of the numerical

results obtained by the present method based on the analytical solution were defined as

$$Error_i = \frac{K_i - K_{i\,exact}}{\sqrt{K^2_{\mathrm{I}\,exact} + K^2_{\mathrm{II}\,exact} + K^2_{\mathrm{III}\,exact}}} \quad (i = \mathrm{I},\ \mathrm{II},\ \mathrm{III}), \tag{53}$$

where $Error_i$ is the relative error (%), and $K_{i\,exact}$ is the analytical solution of the SIF.

The stress intensity factors at $\theta = 45^\circ$ of the crack front (see Fig. 7) calculated by four different radii r of the H-integral path are shown in Table 1. In this example, the error of K_{I} is larger than those of K_{II} and K_{III} because K_{I} is the dominant mode. The obtained stress intensity factors in table 1 show good path-independency and accuracy within 1%.

5.2. A single-edge interfacial corner between dissimilar anisotropic materials

We consider a single edge interfacial corner (a = 2mm, h = 0.18mm) as shown in Fig. 8. The wedge angles of aragonite and GSO are $\alpha = 180^\circ$ and $\beta = 135^\circ$, respectively. The stress intensity factors subjected to a non-uniform change of temperature and a uniform tension σ = 5.0 MPa were analyzed. The change of temperature has a uniform gradient with respect to the X-direction, –25[K/mm]. The material properties of aragonite and GSO are shown in Table 2. The number of nodes and elements of the FE mesh, whose smallest element near the tip was 0.002mm, were 514,458 and 123,876, respectively.

The eigenvalues were $\lambda_{\mathrm{I}} = 0.5010$, $\lambda_{\mathrm{II}} = 0.5306$ and $\lambda_{\mathrm{III}} = 0.6590$. The stress intensity factors at Z = 0.5mm, whose dimensions are related to the smallest eigenvalue λ_{I} are $K_{\mathrm{I}} = 40.94$, $K_{\mathrm{II}} = 50.34$ and $K_{\mathrm{III}} = -1.482\,\mathrm{MPa}\cdot\mathrm{mm}^{0.499}$. By substituting the stress intensity factors obtained by the H-integral into Eq.(47), the stress distribution ahead of an interfacial corner was calculated, where the regular terms were ignored. Excellent agreement between these results and the finite element solutions is shown in Fig. 9, and the accuracy of the stress intensity factors was indirectly demonstrated. Moreover, it can be found that the ratio of stress intensity factors corresponds to the proportion of stress in three deformation modes, qualitatively.

In this case, very fine mesh was used in order to represent accurately the stresses in the vicinity of the corner tip. However, coarser meshes are adequate for the sake of calculating the stress intensity factors.

5.3. A rounded interfacial corner between dissimilar anisotropic materials

An interfacial corner which had a rounded front subjected to a uniform change of temperature –50K as shown in Fig. 10 was analyzed (a = 1mm). The wedge angles of aragonite and GSO are $\alpha = 135^\circ$ and $\beta = 135^\circ$, respectively. The material properties of the respective materials are shown in Table 2. The number of nodes and elements of the FE mesh, whose smallest element near the tip

was 0.1mm, were 375,725 and 90,240, respectively.

Fig. 11 shows the distribution of stress intensity factors along the corner front. The distribution demonstrates complex variation, though it is skew-symmetric with respect to $\theta = 180^{\circ}$. It is an interesting issue how the complex variation of stress intensity factors along a corner front influences the actual fracture from an interfacial corner front.

6. Conclusion

A numerical method using the path-independent *H*-integral based on the conservation integral was developed to analyze the stress intensity factors of a three-dimensional interfacial corner between anisotropic bimaterials under thermal stress. For evaluating the amplitudes of the analyzed singular stress field, a newly proposed definition of the stress intensity factors of an interfacial corner, which involves the smooth expansion of the stress intensity factors of an interfacial crack, was used. Using these stress intensity factors, asymptotic solutions of stress and displacement around an interfacial corner can be uniquely obtained. Using the present method, the analyses of interfacial corners subjected to thermal and mechanical loading were performed and the stress intensity factors were calculated. The calculated stress intensity factors agreed very well with the analytical solutions, and showed good path-independency. And the asymptotic stress solutions obtained by the stress intensity factors showed excellent agreement with the distribution of stress around the anisotropic bimaterial corner which had no analytical solutions. This proved the accuracy of the present method indirectly.

References

Babuska, I., Miller, A., 1984. The post-processing approach in the finite element method —Part 2: the calculation of stress intensity factors. International Journal for Numerical Methods in Engineering 20 (6), 1111-1129.

Banks-Sills, L., 1997. A conservative integral for determining stress intensity factors of a bimaterial strip. International Journal of Fracture 86 (4), 385-398.

Banks-Sills, L., Ishbir, C., 2004. A conservative integral for bimaterial notches subjected to thermal stresses. International Journal for Numerical Methods in Engineering 60 (6),1075-1102.

Barroso, A., Mantic, V. and París, F., 2003. Singularity analysis of anisotropic multimaterial corners. International Journal of Fracture 119, 1-23.

Carpenter, W. C., 1984. Calculation of fracture parameters for a general corner. International Journal of Fracture 24 (1), 45-58.

Carpenter, W. C., Byers. C., 1987. A path independent integral for computing stress intensities for

V-notched cracks in a bi-material. International Journal of Fracture 35 (4), 245-268.

Dempsey, J. P., 1995. Power-logarithmic stress singularities at bi-material corners and interface cracks. Journal of Adhesion Science and Technology 9 (2), 253-265.

Hartranft, R. J. and Sih, G. C., 1969, The use of eigenfunction expansions in the general solution of three-dimensional crack problems. Journal of Mathematics and Mechanics, 19 (2), 123-138.

Hwu, C., 1993, Explicit solutions for collinear interface crack problems. International Journal of Solids and Structures 30 (3), 301-312.

Hwu, C., Omiya, M., Kishimoto, K., 2003. A key matrix N for the stress singularity of the anisotropic elastic composite wedges. JSME International Journal Series A 46 (1), 40-50.

Hwu, C., Kuo, T. L., 2007. A unified definition for stress intensity factors of interface corners and cracks. International Journal of Solids and Structures 44 (18-19), 6340-6359.

Kassir, M. K., Bregman, A. M., 1972. The stress intensity factor for a penny-shaped crack between two dissimilar materials. Journal of Applied Mechanics 39 (1), 308-310.

Labossiere, P. E. W., Dunn, M. L., 1999. Stress intensities at interface corners in anisotropic bimaterials. Engineering Fracture Mechanics 62 (6), 555-575.

Lancaster, P., Salkauskas, K., 1981. Surface generated by moving least squares methods. Mate Comp 37, 141-158.

Nomura, Y., Ikeda, T., Miyazaki, N., 1997, Stress intensity factor at an interfacial corner between anisotropic bimaterials under thermal stress. Engineering Fracture Mechanics 76, 221-235.

Omer, N., Yosibash, Z., Costabel, 2004, M. and Dauge, M., Edge flux intensity functions in polyhedral domains and their extraction by a quasidual function method. International Journal of Fracture 129, 97-130.

Ortiz, J. E., Mantic, V., Paris, F., 2006. A domain-independent integral for computation of stress intensity factors along three-dimensional crack fronts and edges by BEM. International Journal of Solids and Structures 43(18-19), 5593-5612.

Sinclair, G. B., Okajima, M., Griffin, J. H., 1984. Path independent integrals for computing stress intensity factors at sharp corners in elastic plates. International Journal for Numerical Methods in Engineering 20 (6), 999-1008.

Sokolnikoff, I. S., 1956. Mathematical Theory of Elasticity, second ed. McGraw Hill.

Stern, M., Becker, E. B., 1976. Dunham RS. A contour integral computation of mixed-mode stress intensity factors. International Journal of Fracture 12 (3), 359-368.

Stroh, A. N., 1958. Dislocations and cracks in anisotropic elasticity. Philosophical Magazine 3 (30), 625-626.

Szabo, B. A., Babuska, I., 1988. Computation of the amplitude of stress singular terms for cracks

and reentrant corners. ASTM, Philadelphia. STP 969, 101-124.

Ting, T. C. T., 1996. Anisotropic Elasticity: Theory and Application. Oxford University Press, NY.

Yin, W. L., 2003. Anisotropic elasticity and multi-material singularities. Journal of Elasticity 71, 263-292.

Yoshibash, Z., Omer, N., Costabel, M. and Dauge, M., 2005. Edge stress intensity functions in polyhedral domains and their extractions by a quasidual function method. International Journal of Fracture 136, 37-73.

Williams, M. L., 1952. Stress singularities resulting from various boundary conditions in angular corners of plates in extension. Journal of Applied Mechanics 19, 526-528.

Williams, M. L., 1957. On the stress distribution at the base of a stationary crack. Journal of Applied Mechanics 24, 109-114.

Wu, K. C., Chang, F. T., 1993. Near-tip fields in a notched body with dislocations and body forces. Journal of Applied Mechanics 60 (4), 936-941.

Figure captions

Fig. 1 (a) Definition of the local rectangular coordinate system in a 3-D corner front. (b) Geometry of 2-D anisotropic *n*-multibonded materials.

Fig. 2 Schematic of the domain and boundary surfaces.

Fig. 3 Schematic of the *H*-integral contour in a 3-D structure.

Fig. 4 Geometry of an interfacial corner.

Fig. 5 The divided element within the surface integral region.

Fig. 6 The concept of moving least-square method.

Fig. 7 A penny-shaped interfacial crack between semi-infinite dissimilar isotropic materials under uniform tension.

Fig. 8 A single-edge interfacial corner between dissimilar anisotropic materials under non-uniform change of temperature and uniform tension.

Fig. 9 Stress distribution along an aragonite-GSO bimaterial interface.

Fig. 10 A rounded interfacial corner between dissimilar anisotropic materials.

Fig. 11 Distribution of the stress intensity factors along the corner front.

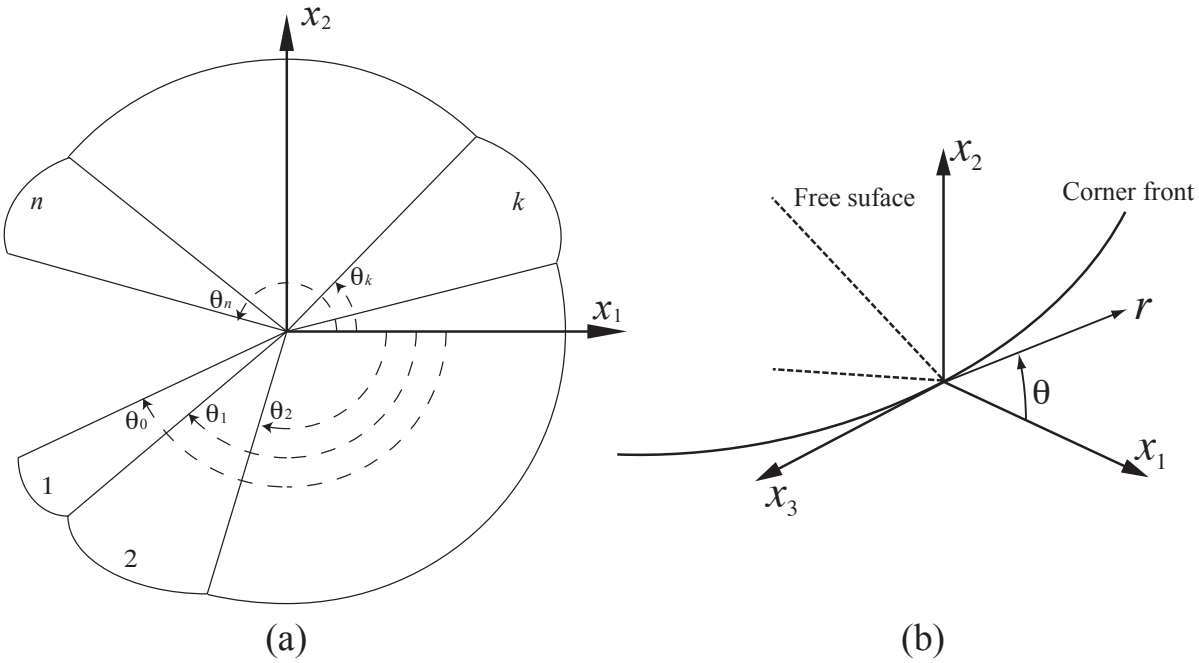

Fig. 1 (a) Definition of the local rectangular coordinate system in a 3-D corner front. (b)Geometry of 2-D anisotropic *n*-multibonded materials.

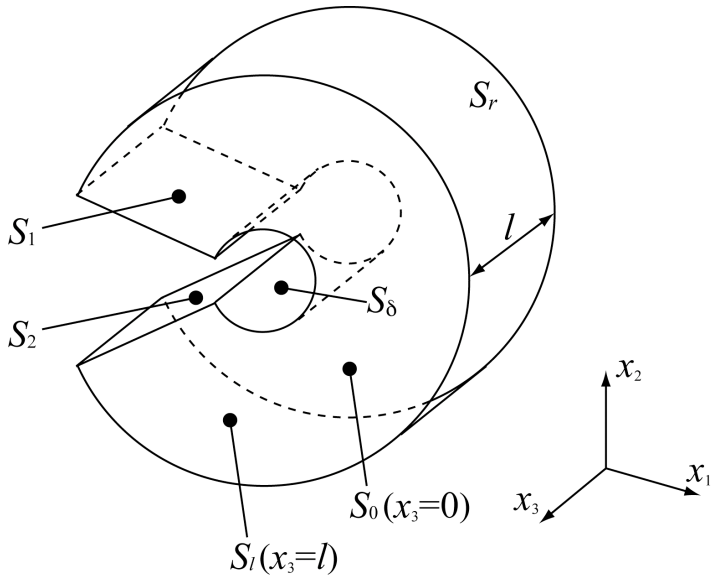

Fig. 2 Schematic of the domain and boundary surfaces.

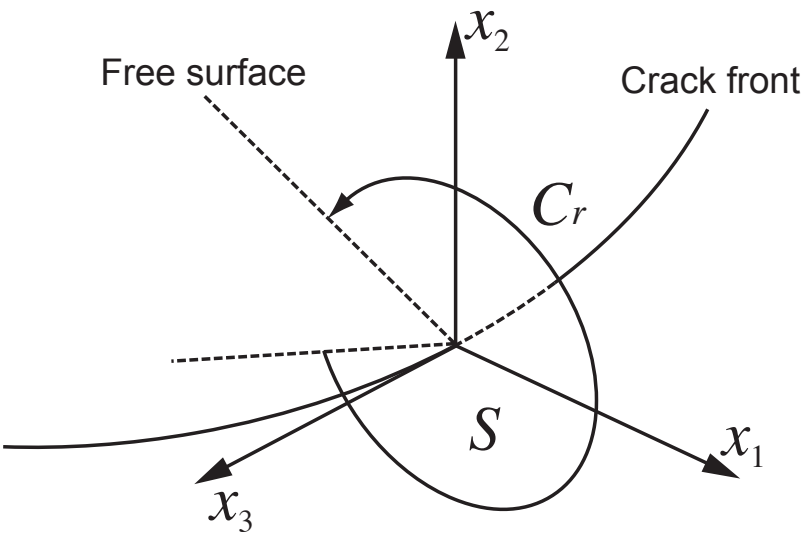

Fig. 3 Schematic of the *H*-integral contour in a 3-D structure.

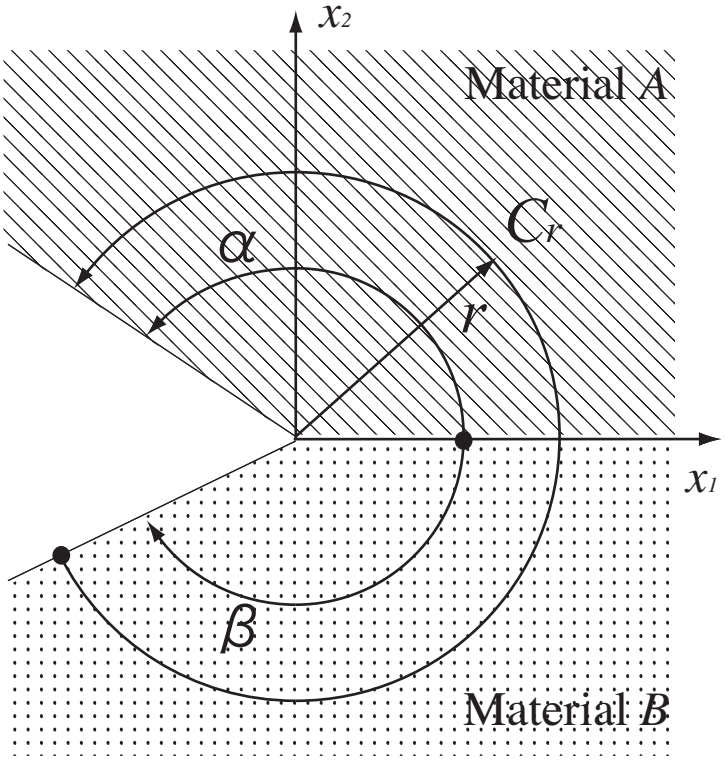

Fig. 4 Geometry of an interfacial corner.

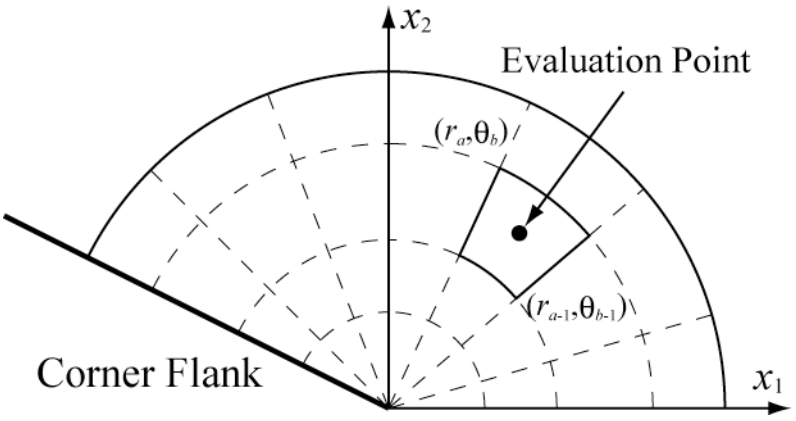

Fig. 5 The divided element within the surface integral region.

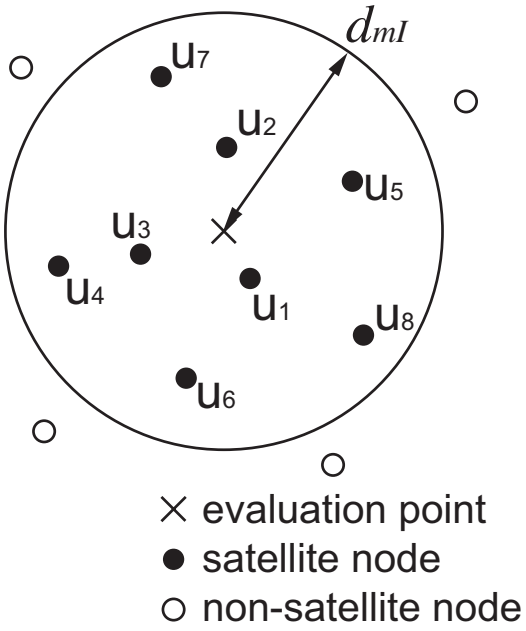

Fig. 6 The concept of moving least-square method.

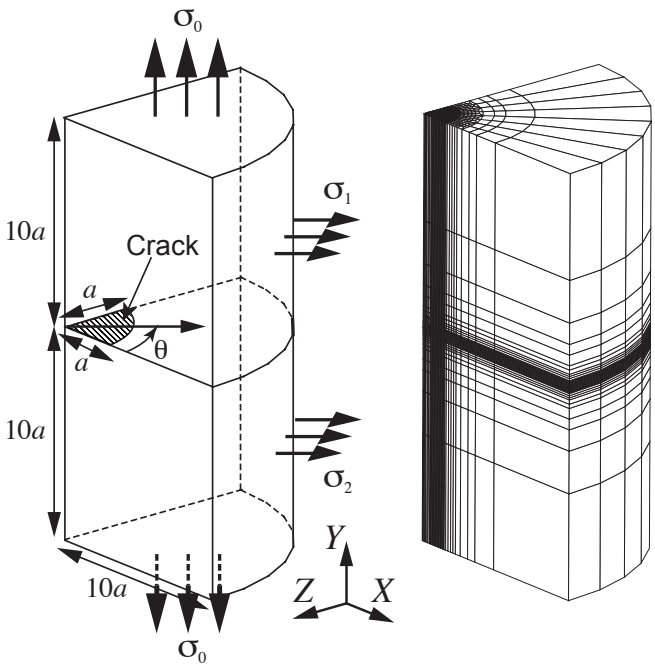

Fig. 7 A penny-shaped interfacial crack between semi-infinite dissimilar isotropic materials under uniform tension.

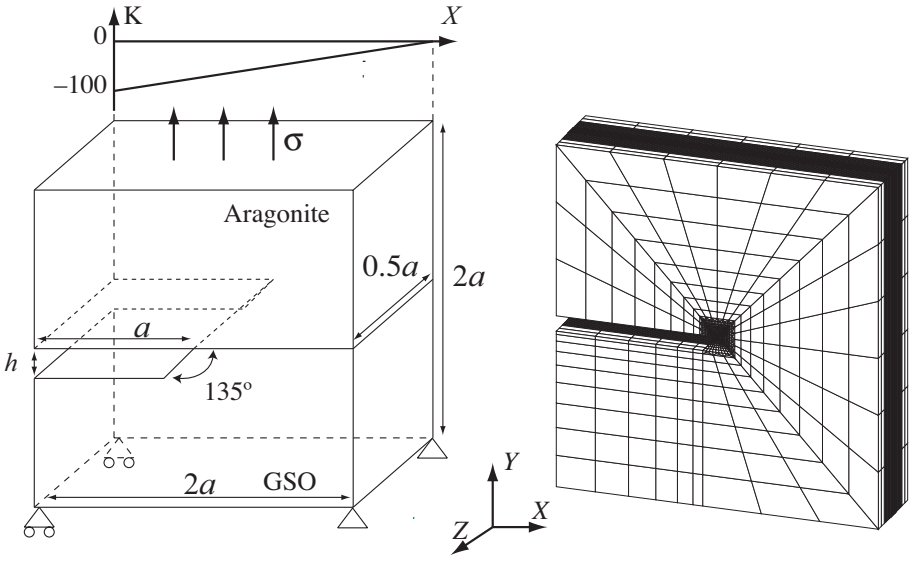

Fig. 8 A single-edge interfacial corner between dissimilar anisotropic materials under non-uniform change of temperature and uniform tension.

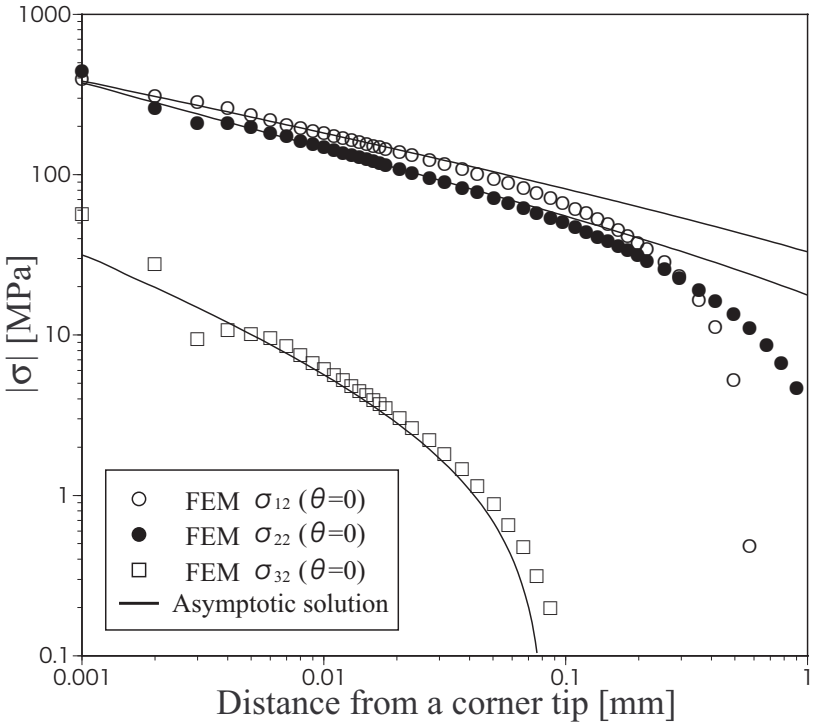

Fig. 9 Stress distribution along an aragonite-GSO bimaterial interface.

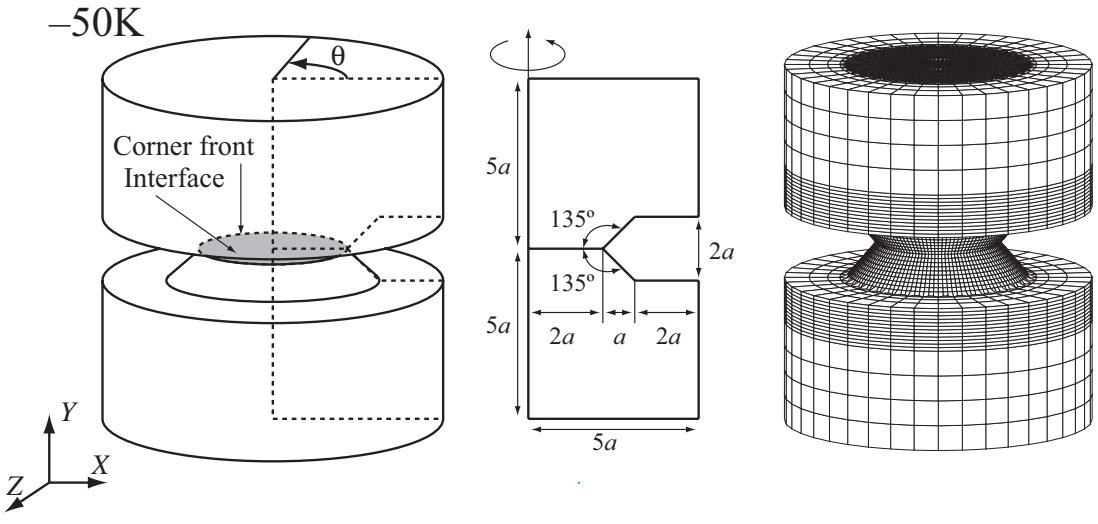

Fig. 10 A rounded interfacial corner between dissimilar anisotropic materials.

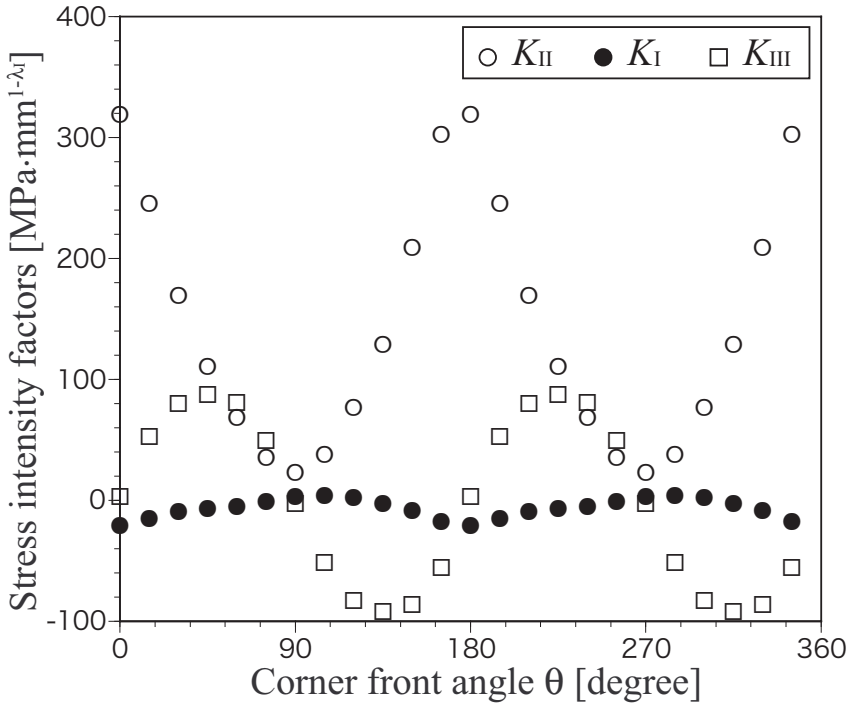

Fig. 11 Distribution of stress intensity factors along the corner front.

Tables

Table 1 Stress intensity factors ($\mathrm{MPa}\sqrt{\mathrm{mm}}$) calculated by four different radii of the *H*-integral path.

r [mm]	K_{II}	K_I	K_{III}
2.0	15.946 (0. 7020%)	32.934 (0.7285%)	-0.0028 (–0.008%)
3.0	15.850 (0. 4553%)	32.870 (0.5629%)	-0.0029 (–0.008%)
4.0	15.834 (0. 4111%)	32.875 (0.5767%)	-0.0028 (–0.008%)
5.0	15.848 (0.4498%)	32.905 (0.6595%)	-0.0029 (–0.008%)
Kassir *et al.* (1972) Translated for l_k= 10μm	15.685	32.666	0.000

Table 2 Elastic stiffness C_{ij} (GPa) and CTE. α_{ij} ($10^{-6}\mathrm{K}^{-1}$) of anisotropic materials.

		Aragonite (Orthotropic)	GSO (Monoclinic)
Elastic Stiffness	C_{11}	160	223
	C_{12}	36.6	108
	C_{13}	1.97	98.5
	C_{15}	0	84
	C_{22}	87	150
	C_{23}	15.9	102
	C_{25}	0	33.3
	C_{33}	85	251
	C_{35}	0	–6
	C_{44}	41.3	78.8
	C_{46}	0	6.6
	C_{55}	25.6	68.8
	C_{66}	42.7	82.7
CTE.	α_{11}	35.0	4.4
	α_{22}	17.0	14.0
	α_{33}	10.0	6.8
	α_{31}	0.0	-1.4